ASTRONOMY

Water heavily fractionated as it ascends on Mars as revealed by ExoMars/NOMAD

Geronimo L. Villanueva[1]*, Giuliano Liuzzi[1,2], Matteo M. J. Crismani[3,4], Shohei Aoki[5,6], Ann Carine Vandaele[4], Frank Daerden[4], Michael D. Smith[1], Michael J. Mumma[1], Elise W. Knutsen[1,2], Lori Neary[5], Sebastien Viscardy[5], Ian R. Thomas[5], Miguel Angel Lopez-Valverde[7], Bojan Ristic[5], Manish R. Patel[8], James A. Holmes[8], Giancarlo Bellucci[9], Jose Juan Lopez-Moreno[7], NOMAD team†

Isotopic ratios and, in particular, the water D/H ratio are powerful tracers of the evolution and transport of water on Mars. From measurements performed with ExoMars/NOMAD, we observe marked and rapid variability of the D/H along altitude on Mars and across the whole planet. The observations (from April 2018 to April 2019) sample a broad range of events on Mars, including a global dust storm, the evolution of water released from the southern polar cap during southern summer, the equinox phases, and a short but intense regional dust storm. In three instances, we observe water at very high altitudes (>80 km), the prime region where water is photodissociated and starts its escape to space. Rayleigh distillation appears the be the driving force affecting the D/H in many cases, yet in some instances, the exchange of water reservoirs with distinctive D/H could be responsible.

INTRODUCTION

Mars shows a scarred landscape carved by a wet past [e.g., (*1*)], yet it is not clear how much of this water ran across the Martian surface or for how long. The debate includes considerations of a wet and cold past scenario [e.g., (*2*)], wet and hot past [e.g., (*3*)], or hybrid models [e.g., (*4*)]. In many cases, these scenarios are stimulated by the strong geological record but depend highly on the assumed atmospheric states and escape considerations. Measurements of isotopic ratios and, in particular, the deuterium to hydrogen ratio (D/H) in water provide a powerful method to constrain volatile escape [e.g., (*5*)] and to track the transport of water between reservoirs (e.g., seasonal transport between the polar caps). Because the thermal "Jeans" escape rates for each isotope are different (larger for the lighter forms), over long periods, the atmosphere becomes enriched in the heavy isotopic forms. By mapping the current isotopic ratios, one can also test for the existence of different volatile reservoirs (e.g., polar caps and regolith) with distinct isotopic signatures (*6*).

The idea of distinct water reservoirs interacting during the water cycle was strengthened by the strong isotopic variations in the water column that were observed across the planet via ground-based astronomy (*5*, *7*). Nevertheless, the D/H ratio is also heavily affected by climatological processes because the vapor pressures of HDO and H_2O differ near the freezing point, making the condensation/sublimation cycle of the isotopologs sensitive to local temperatures, to saturation levels, and to the presence of aerosol condensation nuclei. This would lead to strong seasonal D/H gradients, while local orography and cloud formation would lead to longitudinal variability.

[1]NASA Goddard Space Flight Center, Greenbelt, MD, USA. [2]Department of Physics, American University, Washington, DC, USA. [3]NPP/USRA, Goddard Space Flight Center, Greenbelt, MD, USA. [4]California State University, San Bernardino, Department of Physics, CA USA. [5]Royal Belgian Institute for Space Aeronomy, Brussels, Belgium. [6]University of Liege, Liege, Belgium. [7]Instituto de Astrofísica de Andalucía, Granada, Spain. [8]Open University, Milton Keynes UK. [9]Istituto di Astrofisica e Planetologia, Rome, Italy.
*Corresponding author. Email: geronimo.villanueva@nasa.gov
†See section S2 in the Supplementary Materials.

MATERIALS AND METHODS

By performing high-resolution infrared spectroscopic observations across the entire planet, the ExoMars Trace Gas Orbiter (TGO) provides an unprecedented view of the three-dimensional structure and composition of the Martian atmosphere. Specifically, the NOMAD (Nadir and Occultation for Mars Discovery) (*8*, *9*) instrument suite aboard TGO has the capability to provide vertical profiles and global maps of water (both H_2O and HDO), water ice, and dust using high-resolution infrared spectroscopy. The vertical and seasonal trends in water vapor during the global and regional dust storms of Mars Year (MY) 34 were extensively presented (*10*), while the present work emphasizes the relationship between water abundance and the D/H ratio based on data acquired with the SO (solar occultation) channel of NOMAD between April 2018 (the start of science operations) and April 2019. This interval corresponds to L_s = 162.5° of MY 34 to L_s = 15.0° of MY 35 and included the "global dust storm" (GDS) that engulfed the planet in MY 34 (June to September 2018). A total of 219,464 individual SO spectra through the Martian atmosphere were collected during 1920 occultation events.

ExoMars TGO's near-polar orbit with up to 24 occultations per sol, shared between NOMAD and Atmospheric Chemistry Suite (*11*), permits high-cadence mapping of the variability of water and D/H over time. Sensitivity typically allows water mapping up to an altitude of ~100 km for the main isotopolog of water (H_2O) and up to ~50 km for HDO and, thus, D/H (with a typical resolution of ~1 km), while high opacity from aerosols and airborne dust restrict the lower boundary to 5 to 10 km. The SO channel operates at wavelengths between 2.2 and 4.3 μm (2325 to 4500 cm^{-1}) using an echelle grating, combined with an acousto-optic tunable filter (AOTF) and delivers a spectral resolving power of ~20,000. The width of each AOTF filtered order varies from 20 to 35 cm^{-1}, linearly increasing with the diffraction order number. The infrared channels (SO and nadir channel) of the NOMAD instrument are described in detail in previous works (*12*–*15*), while a complete calibration using the in-flight data acquired before the science phase has been discussed in depth (*16*).

During an occultation, the SO instrument is pointed toward the Sun to observe the solar radiation as attenuated by the Martian atmosphere at different altitudes, enabling an investigation of the atmospheric vertical structure. On a typical occultation, five or six different diffraction orders are sampled at 1-s intervals, with H_2O sampled in two or more diffraction orders and HDO in one of them, ultimately allowing quantification of D/H for almost all NOMAD occultations (see example spectra in Fig. 1). The possibility to access different absorption bands of water is of great benefit to achieve measurement accuracy throughout a vast range of altitudes since absorption regimes vary with the observed atmospheric column. For instance, strong fundamental bands of H_2O (such as the ν_3 band at 2.7 μm, orders 168 to 170) probe water up to 120 km but become saturated at ~50 km, while the weaker $2\nu_2$ band at 3.3 μm (orders 133 to 136) probes deeper into the atmosphere without saturation.

We derived H_2O and HDO slant column densities from the resulting spectra by using Goddard's Planetary Spectrum Generator (PSG) (*17*), which is based on an optimal estimation approach (*18*), modified with an extra regularization parameter (*19*, *20*). For Mars, PSG ingests a specific line compilation for water and its isotopologs, tailored for a CO_2-rich atmosphere (*21*, *22*). The derivation of molecular mixing ratios does depend on the assumed pressure/temperature profiles, and in particular, the local atmospheric density and temperature can vary during perihelion season, depending on the intensity of heating introduced by dust present in the atmosphere. Because portions of the dataset were acquired during the GDS, the a priori atmospheric state has to be representative of those specific conditions. We calculated that using the Global Environmental Multiscale (GEM)–Mars model (*23*, *24*) and a specific dust storm scenario that reproduces the dust state of the atmosphere during MY 34. The properties of the GEM-Mars GDS model during the storm differ substantially from the average climatology of the Mars Climate Database (v5.2) (*25*), with temperature deviations as large as 30 K modeled in the middle atmosphere (fig. S4). The largest discrepancies are found in the southern hemisphere, where dust concentrations are greater during the GDS. The dust abundance or the assumed aerosols profiles do not affect the H_2O and HDO SO retrievals directly (only when the atmosphere is fully optically thick). Dust will tend to heat the atmosphere, and that may reflect in enhanced partition functions, which ultimately affect the retrieved molecular densities. On the other hand, this effect is particularly small for the retrieved D/H since both partition functions vary similarly to temperature, so this systematic effect is removed when computing D/H.

To compute a single molecular profile per occultation, measurements are first collected to form a single dataset colocated in altitude (typically one to two orders for H_2O and one to two orders for HDO) and then aggregated by a weighted mean. Each molecular retrieval is assumed to be independent from the nearby altitude retrievals, with the resulting uncertainty also including the standard deviation of the measurements (see figs. S6 and S7). The D/H ratio is determined using the same approach: For each occultation and altitude, the D/H is computed using the weighted averages of H_2O and HDO. Uncertainties were computed using standard optimal estimation statistics that are further corrected for the quality of the residual spectra (chi-square of the fit). Measurements from several orders and computation of uncertainties of D/H were performed using standard error propagation methods [see also (*5*, *9*)].

RESULTS

The retrievals were organized by season and latitude to investigate the main processes acting on water and D/H. As shown in Fig. 2, the water vapor abundances change markedly across the year, with D/H also showing important changes. Previous measurements of water columns [e.g., (*26*–*30*)] also report great seasonal, temporal, and spatial variability, with strong enhancements during the summer hemisphere as reported here. The seasonal variability reported here should be viewed with caution since the orbit of ExoMars causes seasonal and latitude changes to be convolved (Fig. 2, top). Note that these are local D/H values at a specific altitude (not of the column), and they can be only understood in the context of the local climatology at this specific altitude/latitude/longitude/season.

Consistent with earlier studies of dust storms (*10*, *31*), we found that water vapor abundances in the middle atmosphere (40 to 100 km) increased substantially during the GDS (June to mid-September 2018) and the regional dust storm of January 2019. In particular, water vapor reaches very high altitudes, at least 100 km, during the GDS. A General Circulation Model simulation explained that dust

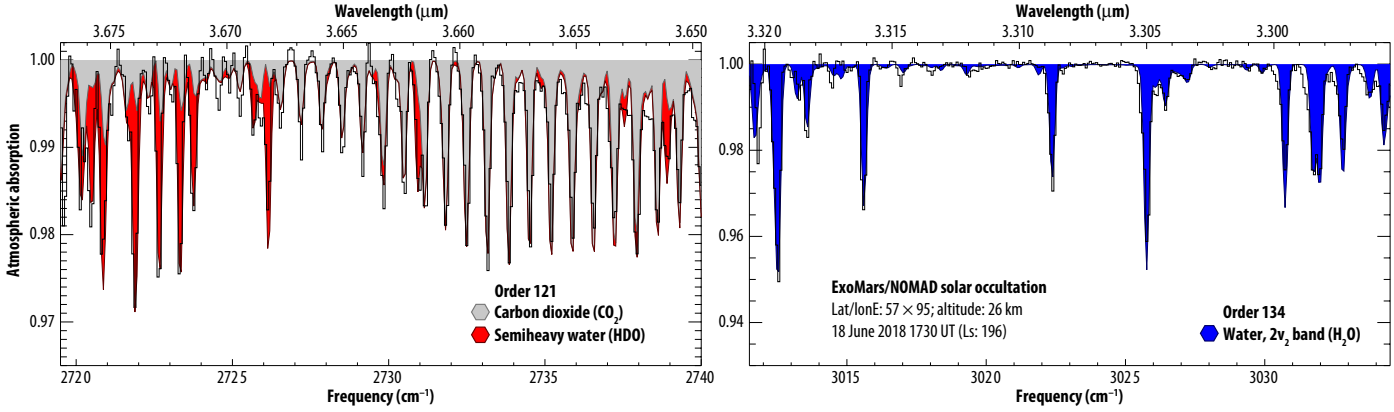

Fig. 1. Representative spectra of the main NOMAD orders used to sample HDO (left) and H_2O (right) taken on June 2018 for a SO altitude of 26 km. The observations were taken during the GDS and show that the two bands (ν_1 of HDO and $2\nu_2$ of H_2O) have similar opacities and, therefore, comparable curves of growth and altitude sensitivity.

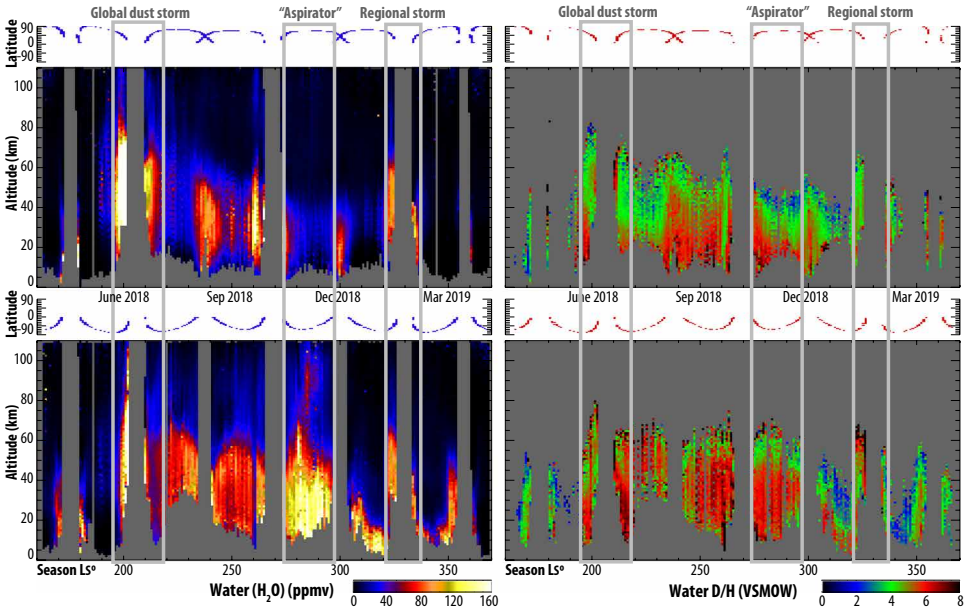

Fig. 2. Seasonal variability of water (left) and the D/H (right) for the northern hemisphere (top) and the southern hemisphere (bottom). Only H_2O values with sigmas lower than 15 parts per million by volume (ppmv) and D/H values with sigmas lower than 0.8 VSMOW are shown (point-by-point error bars are presented in fig. S7). Because of the ExoMars/TGO orbit, there is an intrinsic relationship between the seasonal and latitudinal sampling for the occultations, and the latitude subpanels indicate which latitudes are sampled during a particular instance. Water is observed to reach the upper regions of the atmosphere (>80 km) during indicated events: (i) during the GDS, (ii) during the regional dust storm, and (ii) during southern summer, in which we observe a localized upper atmosphere water excess.

storm–related increases in atmospheric temperatures elevate the hygropause, hence reducing ice cloud formation and so allowing water vapor to extend into the middle atmosphere (*24*). We confirm that (i) water vapor also reaches very high altitudes during the southern summer solstice, independently of dust storms [see lower dust content during this period as reported in (*32*)] and (ii) that water drops to very low values at high/low latitudes and close to equinox with the hygropause subsiding to a few scale heights. With regard to D/H, we observe the following distinct features: (i) the D/H ratio is typically ~6 VSMOW (Vienna Standard Mean Ocean Water) in the lower atmosphere, (ii) the D/H ratio decreases with altitude, as observed similarly on Earth (*22*), and (iii) the D/H ratio is low (2 to 4 VSMOW) at high/low latitudes and close to equinox where H_2O is low.

Within half an MY, we observed three instances (the GDS, southern summer, and the regional dust storm) of water vapor reaching the upper atmosphere, where it can be readily photolyzed (*24*), bypassing the traditional H_2 diffusion limitations on water escape rates (*33*). The D/H ratio is probably quite low at these high altitudes if we attempted to extrapolate our D/H values to 70 to 80 km from the low/middle atmosphere (50 to 60 km), yet photolysis, vertical transport, and other processes may lead to great variability at these altitudes. On Earth, mesospheric D/H measurements show strong variability (*34*), which has been attributed to the differential photolysis rates of HDO and H_2O combined with atmospheric transport and CH_4/CH_3D photochemistry. For the lower atmosphere, the decrease of the D/H with altitude can be explained, as on Earth, by Rayleigh fractionation (*22*). The fractionation in the troposphere of Earth has been shown to be also strongly dependent on atmospheric dynamics [e.g., see convective/subsiding results in (*35*) and formation of clouds and atmospheric microphysics in (*36*)], resulting in highly variable deuterium enrichments with respect to altitude, time, and position on the planet [e.g., (*37*, *38*)]. These may explain the localized behavior and variability in the D/H ratio observed across Mars, and it is consistent with the column variability observed in (*5*).

To explore the 3D structure of the water cycle and the D/H signatures, we aggregated the data into seasonal periods and computed latitude versus altitude plots of water vapor and D/H (Fig. 3). These plots show a marked variability of the vertical profiles of water and D/H, with clear and defined latitudinal structures. As also shown in (*10*), the increase of the water vapor abundances at higher altitudes is remarkable for the global (L_s = 190° to 210°) and regional dust storm (L_s = 320° to 330°), yet this excess water is only confined to equatorial and mid-latitudes (<60°). Although the atmosphere is filled with water to high altitudes during these times, the D/H remains relatively low (4 to 5 VSMOW) and increases to ~6 VSMOW only at high latitudes (away from the subsolar point) and low altitudes. In principle, this is expected and could be an indication of Rayleigh fractionation and cloud formation (*9*), where D/H is actually decreasing with altitude, but it is only measured with sufficient signal-to-noise ratio (low opacities) at high altitudes (>40 km) in mid-latitudes and at low altitudes (10 to 40 km) in high latitudes.

The injection of southern polar cap water with enhanced D/H is clearly seen as southern spring progresses to summer. Between L_s = 270° and 300°, we see water vapor increasing in the southern hemisphere and also in altitude as we approach the polar latitudes [labeled in Fig. 2 as "aspirator" (from the Latin word "aspire" to "rise, climb up")]. The D/H remains high (>6 VSMOW) for most of this water (probably coming from the seasonal southern polar cap) and decreases to <4 VSMOW at higher altitudes. Fractionation is also present at this season, associated with a more compact hygropause in the colder/winter hemisphere and a more compact D/H profile. As we move to southern fall (L_s = 300° to 320°), the water may have been transported

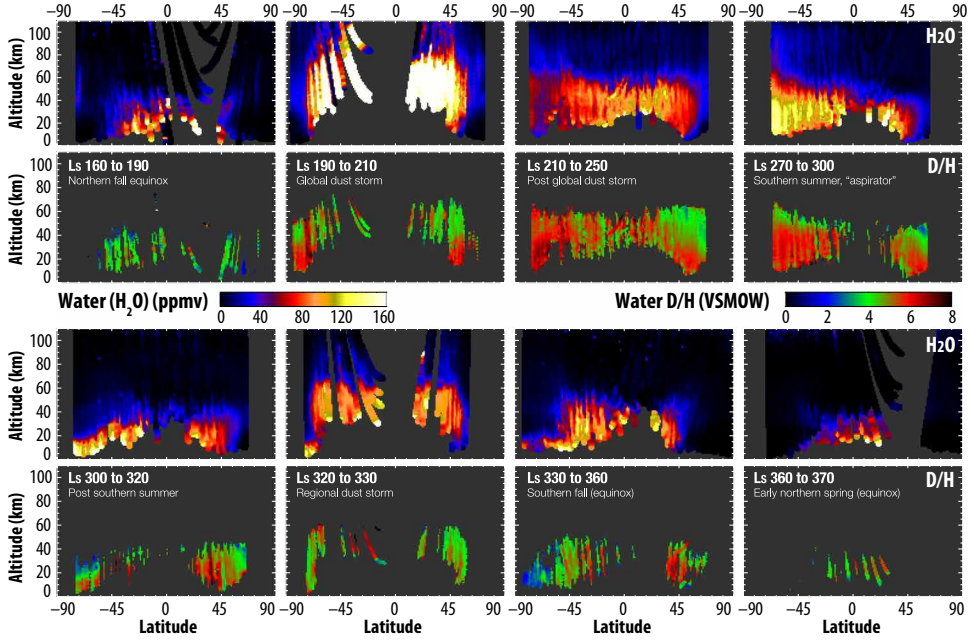

Fig. 3. Latitudinal variability of water and D/H across the seasons, sampling two equinoxes, a solstice, a global and a regional dust storm, and the injection of water into the atmosphere from the southern polar cap during southern summer. Only H_2O values with sigmas lower than 15 ppmv and D/H values with sigmas lower than 1.5 VSMOW are shown. The panels clearly show the evolution of the water cycle across these complex events, revealing marked changes in the water and D/H distributions across the events. The sparsity of valid D/H datasets considering this fine temporal sampling does not allow us to fully capture every detail of the latitude by altitude variability, yet two points are clearly observed: (i) The water released from the southern polar cap has a distinctive 6- to 7-VSMOW enrichment in D/H, and (ii) during southern fall (Ls 300 to 320 and Ls 330 to 360), the hygropause is compacted in the southern hemisphere, leading also to very low D/H at these latitudes and season.

to equatorial latitudes, which is then puffed into higher altitudes during the regional dust storm (L_s = 320° to 330°). During the regional storm, water reaches only 60 km in altitude, in comparison to 80 to 100 km observed during the GDS. Water abundance then collapses to low values and at low altitudes during southern fall (L_s = 330° to 360°) and early northern spring (L_s = 360° to 370°, MY 34). The D/H information during this period is inconclusive since water is confined to low-altitude layers of the atmosphere, where long atmospheric path lengths prevent observations of HDO with sufficient sensitivity due to aerosol extinction. During this season, we do observe low D/H values in the southern hemisphere and very low values at low altitudes.

DISCUSSION

Multiple reservoirs have been identified to account for the current inventory of water on Mars, ranging from the observable polar layered deposits (*39*, *40*) to ice-rich regolith at mid-latitudes (*41*, *42*), near-surface reservoirs at high latitudes (*43*), and subsurface reservoirs, as implied by gamma ray and neutron observations (*44*). If each of these reservoirs has a distinct isotopic content, then the signature of the exchange between these reservoirs should be present in the observed atmospheric D/H ratio variation. The outstanding question is whether each reservoir has or should have a distinct isotopic signature. The fact that Mars has had marked variations in its obliquity (*45*), changing from ~45° to 15° in the last million years, would suggest that the polar caps are relatively new and that all the water reservoirs should have been "mixed" within the last 10 million years. Considering that it takes billions of years for notable changes in the D/H ratio to take effect, the different reservoirs may have the same isotopic signature, yet this hypothesis assumes that all labile water is mixed by the hydrological cycle. A testable way to prove this hypothesis would be to ultimately probe the water D/H in the polar caps below the seasonal layers. We then ask, is the variability that we observe related to different reservoirs?

As on Earth (*46*), D/H on Mars shows great variability in time and space, consistent with previous column integrated reports in (*5*, *47*). Observations using SOFIA (Stratospheric Observatory for Infrared Astronomy) at thermal wavelengths (*48*) do also report variability yet much more subdued. Thermal observations are more affected by the assumed temperature profiles and thermal contrast, and the spatial resolution of SOFIA observations is typically only four to five pixels across Mars' disk; however, it is interesting to note this difference between SOFIA and other results. In particular, there may be an annual element to this hemispheric variability of the observed D/H column. Strong isotopic anomalies are typically observed at regions with strong temperature/water gradients, like the polar caps, and these are typically hard to capture and sample at moderate spatial resolutions from the ground.

In many cases, the observed variations of the D/H across seasons and with altitude revealed by our work could be attributed to Rayleigh fractionation and cloud formation (*32*), with the D/H decreasing with altitude and dropping or decreasing at the edge of the hygropause. In the zonal mean Fig. 3, the seasonal water being added from the southern polar cap during southern summer (L_s = 210° to 250° and 270° to 300°) has a ~6- to 7-VSMOW value, consistent with the column values measured in (*5*) for the northern pole water. This would perhaps mean that the two main reservoirs of water on Mars,

the polar caps, share a common value of D/H, yet the south polar cap only has seasonal water ice, not permanent. The lower values in D/H observed during southern fall (L_s = 300° to 320° and 330° to 360°) at the southern latitudes would imply that a large fraction of the HDO was sequestered. This could be associated to be a rapid collapse of the hygropause at these latitudes, which leads to a steep Rayleigh fractionation condensation profile. The existence of water ice clouds during this period and season (*31*, *32*) is consistent with this view.

Further interpreting the results, in particular, the concept of multiple reservoirs of water with a distinctive D/H and water escape would require detailed comparisons with a highly parameterized weather and climate model. The model would need to have a comparable prescription of the water and aerosol distribution and to have a realistic heterogenous water fractionation model to fully capture the observed D/H variability and advance current models (*49*–*51*). The ultimate question is then what is the representative D/H of labile water on Mars right now? If we assume that the observed fractionation is driven mainly by Rayleigh distillation, then the observed maximum D/H values of 6 to 7 VSMOW observed in this work are then descriptive of the truly intrinsic water D/H when both isotopologs are fully vaporized. This value is consistent with previous findings as reported above and would further establish that Mars has lost a substantial amount of water (>137-m global equivalent layer) (*5*). The fact that we observe three instances during a single MY where water is brought to the upper regions of the atmosphere (>60 km; Figs. 2 and 3) would provide the means for this escape to take place.

SUPPLEMENTARY MATERIALS

Supplementary material for this article is available at http://advances.sciencemag.org/cgi/content/full/7/7/eabc8843/DC1

REFERENCES AND NOTES

1. M. H. Carr, J. W. Head III, Oceans on Mars: An assessment of the observational evidence and possible fate. *J. Geophys. Res.* **108**, 5042 (2003).
2. A. G. Fairén, A cold and wet Mars. *Icarus* **208**, 165–175 (2010).
3. J. M. Davis, M. Balme, P. M. Grindrod, R. M. E. Williams, S. Gupta, Extensive Noachian fluvial systems in Arabia Terra: Implications for early Martian climate. *Geology* **44**, 847–850 (2016).
4. K. M. Cannon, S. W. Parman, J. F. Mustard, Primordial clays on Mars formed beneath a steam or supercritical atmosphere. *Nature* **552**, 88–91 (2017).
5. G. L. Villanueva, M. J. Mumma, R. E. Novak, H. U. Käufl, P. Hartogh, T. Encrenaz, A. Tokunaga, A. Khayat, M. D. Smith, Strong water isotopic anomalies in the martian atmosphere: Probing current and ancient reservoirs. *Science* **348**, 218–221 (2015).
6. D. Fisher, R. E. Novak, M. J. Mumma, D/H ratio during the northern polar summer and what the Phoenix mission might measure. *J. Geophys. Res.* **113**, E00A15 (2008).
7. R. E. Novak, M. J. Mumma, G. L. Villanueva, Measurement of the isotopic signatures of water on Mars; implications for studying methane. *Planet. Space Sci.* **59**, 163–168 (2011).
8. A. C. Vandaele, J. J. López-Moreno, M. R. Patel, G. Bellucci, F. Daerden, R. Drummond, E. Neefs, S. Robert, J. Rodriguez Gomez, NOMAD, a spectrometer suite for nadir and solar occultation observations on the ExoMars Trace Gas Orbiter. *EGU Gen. Assem. 2012* **14**, 3362 (2012).
9. A. C. Vandaele, O. Korablev, F. Daerden, S. Aoki, I. R. Thomas, F. Altieri, M. López-Valverde, G. Villanueva, G. Liuzzi, M. D. Smith, J. T. Erwin, L. Trompet, A. A. Fedorova, F. Montmessin, A. Trokhimovskiy, D. A. Belyaev, N. I. Ignatiev, M. Luginin, K. S. Olsen, L. Baggio, J. Alday, J.-L. Bertaux, D. Betsis, D. Bolsée, R. T. Clancy, E. Cloutis, C. Depiesse, B. Funke, M. Garcia-Comas, J.-C. Gérard, M. Giuranna, F. Gonzalez-Galindo, A. V. Grigoriev, Y. S. Ivanov, J. Kaminski, O. Karatekin, F. Lefèvre, S. Lewis, M. López-Puertas, A. Mahieux, I. Maslov, J. Mason, M. J. Mumma, L. Neary, E. Neefs, A. Patrakeev, D. Patsaev, B. Ristic, S. Robert, F. Schmidt, A. Shakun, N. A. Teanby, S. Viscardy, Y. Willame, J. Whiteway, V. Wilquet, M. J. Wolff, G. Bellucci, M. R. Patel, J.-J. López-Moreno, F. Forget, C. F. Wilson, H. Svedhem, J. L. Vago, D. Rodionov; NOMAD Science Team; ACS Science Team, Martian dust storm impact on atmospheric H_2O and D/H observed by ExoMars Trace Gas Orbiter. *Nature* **568**, 521–525 (2019).
10. S. Aoki, A. C. Vandaele, F. Daerden, G. L. Villanueva, G. Liuzzi, I. R. Thomas, J. T. Erwin, L. Trompet, S. Robert, L. Neary, S. Viscardy, R. T. Clancy, M. D. Smith, M. A. Lopez-Valverde, B. Hill, B. Ristic, M. R. Patel, G. Bellucci, J.-J. Lopez-Moreno; NOMAD Team, Water vapor vertical profiles on Mars in dust storms observed by TGO/NOMAD. *J. Geophys. Res. Planets* **124**, 3482–3497 (2019).
11. O. Korablev, F. Montmessin, A. Trokhimovskiy, A. A. Fedorova, A. V. Shakun, A. V. Grigoriev, B. E. Moshkin, N. I. Ignatiev, F. Forget, F. Lefèvre, K. Anufreychik, I. Dzuban, Y. S. Ivanov, Y. K. Kalinnikov, T. O. Kozlova, A. Kungurov, V. Makarov, F. Martynovich, I. Maslov, D. Merzlyakov, P. P. Moiseev, Y. Nikolskiy, A. Patrakeev, D. Patsaev, A. Santos-Skripko, O. Sazonov, N. Semena, A. Semenov, V. Shashkin, A. Sidorov, A. V. Stepanov, I. Stupin, D. Timonin, A. Y. Titov, A. Viktorov, A. Zharkov, F. Altieri, G. Arnold, D. A. Belyaev, J. L. Bertaux, D. S. Betsis, N. Duxbury, T. Encrenaz, T. Fouchet, J.-C. Gérard, D. Grassi, S. Guerlet, P. Hartogh, Y. Kasaba, I. Khatuntsev, V. A. Krasnopolsky, R. O. Kuzmin, E. Lellouch, M. A. Lopez-Valverde, M. Luginin, A. Määttänen, E. Marcq, J. Martin Torres, A. S. Medvedev, E. Millour, K. S. Olsen, M. R. Patel, C. Quantin-Nataf, A. V. Rodin, V. I. Shematovich, I. Thomas, N. Thomas, L. Vazquez, M. Vincendon, V. Wilquet, C. F. Wilson, L. V. Zasova, L. M. Zelenyi, M. P. Zorzano, The Atmospheric Chemistry Suite (ACS) of three spectrometers for the ExoMars 2016 trace gas orbiter. *Space Sci. Rev.* **214**, 7 (2018).
12. A. C. Vandaele, E. Neefs, R. Drummond, I. R. Thomas, F. Daerden, J.-J. Lopez-Moreno, J. Rodriguez, M. R. Patel, G. Bellucci, M. Allen, F. Altieri, D. Bolsée, T. Clancy, S. Delanoye, C. Depiesse, E. Cloutis, A. Fedorova, V. Formisano, B. Funke, D. Fussen, A. Geminale, J.-C. Gérard, M. Giuranna, N. Ignatiev, J. Kaminski, O. Karatekin, F. Lefèvre, M. López-Puertas, M. López-Valverde, A. Mahieux, J. McConnell, M. Mumma, L. Neary, E. Renotte, B. Ristic, S. Robert, M. Smith, S. Trokhimovsky, J. V. Auwera, G. Villanueva, J. Whiteway, V. Wilquet, M. Wolff, Science objectives and performances of NOMAD, a spectrometer suite for the ExoMars TGO mission. *Planet. Space Sci.* **119**, 233–249 (2015).
13. A. C. Vandaele, J.-J. Lopez-Moreno, M. R. Patel, G. Bellucci, F. Daerden, B. Ristic, S. Robert, I. R. Thomas, V. Wilquet, M. Allen, G. Alonso-Rodrigo, F. Altieri, S. Aoki, D. Bolsée, T. Clancy, E. Cloutis, C. Depiesse, R. Drummond, A. Fedorova, V. Formisano, B. Funke, F. González-Galindo, A. Geminale, J.-C. Gérard, M. Giuranna, L. Hetey, N. Ignatiev, J. Kaminski, O. Karatekin, Y. Kasaba, M. Leese, F. Lefèvre, S. R. Lewis, M. López-Puertas, M. López-Valverde, A. Mahieux, J. Mason, J. McConnell, M. Mumma, L. Neary, E. Neefs, E. Renotte, J. Rodriguez-Gomez, G. Sindoni, M. Smith, A. Stiepen, A. Trokhimovsky, J. V. Auwera, G. Villanueva, S. Viscardy, J. Whiteway, Y. Willame, M. Wolff, NOMAD, an integrated suite of three spectrometers for the ExoMars trace gas mission: Technical description, science objectives and expected performance. *Space Sci. Rev.* **214**, 80 (2018).
14. E. Neefs, A. C. Vandaele, R. Drummond, I. R. Thomas, S. Berkenbosch, R. Clairquin, S. Delanoye, B. Ristic, J. Maes, S. Bonnewijn, G. Pieck, E. Equeter, C. Depiesse, F. Daerden, E. V. Ransbeeck, D. Nevejans, J. Rodriguez-Gómez, J.-J. López-Moreno, R. Sanz, R. Morales, G. P. Candini, M. C. Pastor-Morales, B. A. del Moral, J.-M. Jeronimo-Zafra, J. M. Gómez-López, G. Alonso-Rodrigo, I. Pérez-Grande, J. Cubas, A. M. Gomez-Sanjuan, F. Navarro-Medina, T. Thibert, M. R. Patel, G. Bellucci, L. De Vos, S. Lesschaeve, N. V. Vooren, W. Moelans, L. Aballea, S. Glorieux, A. Baeke, D. Kendall, J. De Neef, A. Soenen, P.-Y. Puech, J. Ward, J.-F. Jamoye, D. Diez, A. Vicario-Arroyo, M. Jankowski, NOMAD spectrometer on the ExoMars trace gas orbiter mission: Part 1—Design, manufacturing and testing of the infrared channels. *Appl. Optics* **54**, 8494–8520 (2015).
15. I. R. Thomas, A. C. Vandaele, S. Robert, E. Neefs, R. Drummond, F. Daerden, S. Delanoye, B. Ristic, S. Berkenbosch, R. Clairquin, J. Maes, S. Bonnewijn, C. Depiesse, A. Mahieux, L. Trompet, L. Neary, Y. Willame, V. Wilquet, D. Nevejans, L. Aballea, W. Moelans, L. De Vos, S. Lesschaeve, N. Van Vooren, J.-J. Lopez-Moreno, M. R. Patel, G. Bellucci; NOMAD Team, Optical and radiometric models of the NOMAD instrument part II: The infrared channels – SO and LNO. *Opt. Express* **24**, 3790–3805 (2016).
16. G. Liuzzi, G. L. Villanueva, M. J. Mumma, M. D. Smith, F. Daerden, B. Ristic, I. Thomas, A. C. Vandaele, M. R. Patel, J.-J. Lopez-Moreno, G. Bellucci, Methane on Mars: New insights into the sensitivity of CH4 with the NOMAD/ExoMars spectrometer through its first in-flight calibration. *Icarus* **321**, 671–690 (2019).
17. G. L. Villanueva, M. D. Smith, S. Protopapa, S. Faggi, A. M. Mandell, Planetary spectrum generator: An accurate online radiative transfer suite for atmospheres, comets, small bodies and exoplanets. *J. Quant. Spectrosc. Radiat. Transf.* **217**, 86–104 (2018).
18. C. D. Rodgers, *Inverse Methods for Atmospheric Sounding* (series on Atmospheric, Oceanic and Planetary Physics, World Scientific, 2000); www.worldscientific.com/worldscibooks/10.1142/3171.
19. G. Liuzzi, G. Masiello, C. Serio, S. Venafra, C. Camy-Peyret, Physical inversion of the full IASI spectra: Assessment of atmospheric parameters retrievals, consistency of spectroscopy and forward modelling. *J. Quant. Spectrosc. Radiat. Transf.* **182**, 128–157 (2016).
20. A. Carissimo, I. De Feis, C. Serio, The physical retrieval methodology for IASI: The δ-IASI code. *Environ. Model. Software* **20**, 1111–1126 (2005).
21. I. E. Gordon, L. S. Rothman, C. Hill, R. V. Kochanov, Y. Tan, P. F. Bernath, M. Birk, V. Boudon, A. Campargue, K. V. Chance, B. J. Drouin, J.-M. Flaud, R. R. Gamache, J. T. Hodges, D. Jacquemart, V. I. Perevalov, A. Perrin, K. P. Shine, M. A. H. Smith, J. Tennyson, G. C. Toon, H. Tran, V. G. Tyuterev, A. Barbe, A. G. Császár, V. M. Devi, T. Furtenbacher,

J. J. Harrison, J.-M. Hartmann, A. Jolly, T. J. Johnson, T. Karman, I. Kleiner, A. A. Kyuberis, J. Loos, O. M. Lyulin, S. T. Massie, S. N. Mikhailenko, N. Moazzen-Ahmadi, H. S. P. Müller, O. V. Naumenko, A. V. Nikitin, O. L. Polyansky, M. Rey, M. Rotger, S. W. Sharpe, K. Sung, E. Starikova, S. A. Tashkun, J. V. Auwera, G. Wagner, J. Wilzewski, P. Wcislo, S. Yu, E. J. Zak, The HITRAN2016 molecular spectroscopic database. *J. Quant. Spectrosc. Radiat. Transf.* **203**, 3–69 (2017).

22. G. L. Villanueva, M. J. Mumma, B. P. Bonev, R. E. Novak, R. J. Barber, M. A. DiSanti, Water in planetary and cometary atmospheres: H_2O/HDO transmittance and fluorescence models. *J. Quant. Spectrosc. Radiat. Transf.* **113**, 202–220 (2012).
23. F. Daerden, L. Neary, S. Viscardy, A. García Muñoz, R. T. Clancy, M. D. Smith, T. Encrenaz, A. Fedorova, Mars atmospheric chemistry simulations with the GEM-Mars general circulation model. *Icarus* **326**, 197–224 (2019).
24. L. Neary, F. Daerden, S. Aoki, J. Whiteway, R. T. Clancy, M. Smith, S. Viscardy, J. T. Erwin, I. R. Thomas, G. Villanueva, G. Liuzzi, M. Crismani, M. Wolff, S. R. Lewis, J. A. Holmes, M. R. Patel, M. Giuranna, C. Depiesse, A. Piccialli, S. Robert, L. Trompet, Y. Willame, B. Ristic, A. C. Vandaele, Explanation for the increase in high altitude water on Mars observed by NOMAD during the 2018 global dust storm. *Geophys. Res. Lett.* **47**, e2019GL084354 (2019).
25. E. Millour, F. Forget, A. Spiga, T. Navarro, J.-B. Madeleine, L. Montabone, A. Pottier, F. Lefevre, F. Montmessin, J.-Y. Chaufray, M. A. Lopez-Valverde, F. Gonzalez-Galindo, S. R. Lewis, P. L. Read, J.-P. Huot, M.-C. Desjean; MCD/GCM development Team, The Mars Climate Database (MCD version 5.2). *Eur. Planet. Sci. Congr.* **10**, EPSC2015-438 (2015).
26. B. M. Jakosky, C. B. Farmer, The seasonal and global behavior of water vapor in the Mars atmosphere: Complete global results of the Viking atmospheric water detector experiment. *J. Geophys. Res.* **87**, 2999–3019 (1982).
27. M. D. Smith, Interannual variability in TES atmospheric observations of Mars during 1999–2003. *Icarus* **167**, 148–165 (2004).
28. M. D. Smith, Spacecraft observations of the martian atmosphere. *Annu. Rev. Earth Planet. Sci.* **36**, 191–219 (2008).
29. F. Montmessin, M. D. Smith, Y. Langevin, M. T. Mellon, A. Fedorova, The water cycle. *Atmos. Clim. Mars*, 338–373 (2017).
30. M. D. Smith, F. Daerden, L. Neary, A. Khayat, The climatology of carbon monoxide and water vapor on Mars as observed by CRISM and modeled by the GEM-Mars general circulation model. *Icarus* **301**, 117–131 (2018).
31. A. A. Fedorova, F. Montmessin, O. Korablev, M. Luginin, A. Trokhimovskiy, D. A. Belyaev, N. I. Ignatiev, F. Lefèvre, J. Alday, P. G. J. Irwin, K. S. Olsen, J.-L. Bertaux, E. Millour, A. Määttänen, A. Shakun, A. V. Grigoriev, A. Patrakeev, S. Korsa, N. Kokonkov, L. Baggio, F. Forget, C. F. Wilson, Stormy water on Mars: The distribution and saturation of atmospheric water during the dusty season. *Science* **367**, 297–300 (2020).
32. G. Liuzzi, G. L. Villanueva, M. M. J. Crismani, M. D. Smith, M. J. Mumma, F. Daerden, S. Aoki, A. C. Vandaele, R. T. Clancy, J. Erwin, I. Thomas, B. Ristic, J.-J. Lopez-Moreno, G. Bellucci, M. R. Patel, Strong variability of martian water ice clouds during dust storms revealed from ExoMars Trace Gas Orbiter/NOMAD. *J. Geophys. Res. Planets* **125**, 2019JE006250 (2020).
33. M. S. Chaffin, J. Deighan, N. M. Schneider, A. I. F. Stewart, Elevated atmospheric escape of atomic hydrogen from Mars induced by high-altitude water. *Nat. Geosci.* **10**, 174–178 (2017).
34. B. J. Sandor, R. T. Clancy, HDO in the mesosphere: Observation and modeling of novel isotopic variability. *J. Geophys. Res.* **108**, 4463 (2003).
35. P. N. Blossey, Z. Kuang, D. M. Romps, Isotopic composition of water in the tropical tropopause layer in cloud-resolving simulations of an idealized tropical circulation. *J. Geophys. Res.* **115**, 24309 (2010).
36. A. Gettelman, C. R. Webster, Simulations of water isotope abundances in the upper troposphere and lower stratosphere and implications for stratosphere troposphere exchange. *J. Geophys. Res.* **110**, 17301 (2005).
37. C. Frankenberg, K. Yoshimura, T. Warneke, I. Aben, A. Butz, N. Deutscher, D. Griffith, F. Hase, J. Notholt, M. Schneider, H. Schrijver, T. Rockmann, Dynamic processes governing lower-tropospheric HDO/H_2O Ratios as observed from space and ground. *Science* **325**, 1374–1377 (2009).
38. W. J. Randel, E. Moyer, M. Park, E. Jensen, P. Bernath, K. Walker, C. Boone, Global variations of HDO and HDO/H_2O ratios in the upper troposphere and lower stratosphere derived from ACE-FTS satellite measurements. *J. Geophys. Res. Atmos.* **117**, D06303 (2012).
39. J. J. Plaut, G. Picardi, A. Safaeinili, A. B. Ivanov, S. M. Milkovich, A. Cicchetti, W. Kofman, J. Mouginot, W. M. Farrell, R. J. Phillips, S. M. Clifford, A. Frigeri, R. Orosei, C. Federico, I. P. Williams, D. A. Gurnett, E. Nielsen, T. Hagfors, E. Heggy, E. R. Stofan, D. Plettemeier, T. R. Watters, C. J. Leuschen, P. Edenhofer, Subsurface radar sounding of the south polar layered deposits of Mars. *Science* **316**, 92–95 (2007).
40. M. T. Zuber, D. E. Smith, S. C. Solomon, J. B. Abshire, R. S. Afzal, O. Aharonson, K. Fishbaugh, P. G. Ford, H. V. Frey, J. B. Garvin, J. W. Head, A. B. Ivanov, C. L. Johnson, D. O. Muhleman, G. A. Neumann, G. H. Pettengill, R. J. Phillips, X. Sun, H. J. Zwally, W. B. Banerdt, T. C. Duxbury, Observations of the north polar region of Mars from the Mars orbiter laser altimeter. *Science* **282**, 2053–2060 (1998).
41. J. B. Murray, J.-P. Muller, G. Neukum, S. C. Werner, S. Van Gasselt, E. Hauber, W. J. Markiewicz, J. W. Head III, B. H. Foing, D. Page, K. L. Mitchell, G. Portyankina; HRSC Co-Investigator Team, Evidence from the Mars express high resolution stereo camera for a frozen sea close to Mars' equator. *Nature* **434**, 352–356 (2005).
42. D. P. Page, M. R. Balme, M. M. Grady, Dating martian climate change. *Icarus* **203**, 376–389 (2009).
43. P. H. Smith, L. K. Tamppari, R. E. Arvidson, D. Bass, D. Blaney, W. V. Boynton, A. Carswell, D. C. Catling, B. Clark, T. Duck, E. DeJong, D. Fisher, W. Goetz, H. P. Gunnlaugsson, M. H. Hecht, V. Hipkin, J. Hoffman, S. F. Hviid, H. U. Keller, S. P. Kounaves, C. F. Lange, M. T. Lemmon, M. B. Madsen, W. J. Markiewicz, J. Marshall, C. P. McKay, M. T. Mellon, D. W. Ming, R. V. Morris, W. T. Pike, N. Renno, U. Staufer, C. Stoker, P. Taylor, J. A. Whiteway, A. P. Zent, H_2O at the Phoenix landing site. *Science* **325**, 58–61 (2009).
44. W. V. Boynton, W. C. Feldman, S. W. Squyres, T. H. Prettyman, J. Brückner, L. G. Evans, R. C. Reedy, R. Starr, J. R. Arnold, D. M. Drake, P. A. J. Englert, A. E. Metzger, I. Mitrofanov, J. I. Trombka, C. d'Uston, H. Wänke, O. Gasnault, D. K. Hamara, D. M. Janes, R. L. Marcialis, S. Maurice, I. Mikheeva, G. J. Taylor, R. Tokar, C. Shinohara, Distribution of hydrogen in the near surface of Mars: Evidence for subsurface ice deposits. *Science* **297**, 81–85 (2002).
45. J. Laskar, A. C. M. Correia, M. Gastineau, F. Joutel, B. Levrard, P. Robutel, Long term evolution and chaotic diffusion of the insolation quantities of Mars. *Icarus* **170**, 343–364 (2004).
46. W. Darling, G, A. H. Bath, J. J. Gibson, K. Rozanski, Isotopes in water, in *Isotopes in Palaeoenvironmental Research*, M. J. Leng, Ed. (Springer, 2006), pp. 1–66.
47. A. S. J. Khayat, G. L. Villanueva, M. D. Smith, S. D. Guzewich, IRTF/CSHELL mapping of atmospheric HDO, H_2O and D/H on Mars during northern summer. *Icarus* **330**, 204–216 (2019).
48. T. Encrenaz, C. DeWitt, M. J. Richter, T. K. Greathouse, T. Fouchet, F. Montmessin, F. Lefèvre, B. Bézard, S. K. Atreya, S. Aoki, H. Sagawa, New measurements of D/H on Mars using EXES aboard SOFIA. *Astron. Astrophys.* **612**, A112 (2018).
49. F. Montmessin, T. Fouchet, F. Forget, Modeling the annual cycle of HDO in the Martian atmosphere. *J. Geophys. Res.* **110**, 03006 (2005).
50. F. Daerden, L. Neary, S. Viscardy, S. Aoki, A. Piccialli, S. Robert, V. Wilquet, I. Thomas, B. Ristic, A. Carine Vandaele, G. Villanueva, M. Mumma, R. Novak, T. Encrenaz, S. Lewis, J. Holmes, J. Juan López-Moreno, G. Bellucci, M. Patel, Model expectations for the D/H distribution on Mars as observed by NOMAD. *Eur. Planet. Sci. Congr.* **12**, EPSC2018-742 (2018).
51. R. Hu, Predicted diurnal variation of the deuterium to hydrogen ratio in water at the surface of Mars caused by mass exchange with the regolith. *Earth Planet. Sci. Lett.* **519**, 192–201 (2019).
52. D. Nevejans, E. Neefs, E. Van Ransbeeck, S. Berkenbosch, R. Clairquin, L. De Vos, W. Moelans, S. Glorieux, A. Baeke, O. Korablev, Compact high-resolution spaceborne echelle grating spectrometer with acousto-optical tunable filter based order sorting for the infrared domain from 2.2 to 4.3 μm. *Appl. Optics* **45**, 5191–5206 (2006).
53. A. Mahieux, S. Berkenbosch, R. Clairquin, D. Fussen, N. Mateshvili, E. Neefs, D. Nevejans, B. Ristic, A. C. Vandaele, V. Wilquet, In-flight performance and calibration of SPICAV SOIR onboard Venus Express. *Appl. Optics* **47**, 2252–2265 (2008).
54. M. D. Smith, M. J. Wolff, R. T. Clancy, A. Kleinböhl, S. L. Murchie, Vertical distribution of dust and water ice aerosols from CRISM limb-geometry observations. *J. Geophys. Res. Planets.* **118**, 321–334 (2013).
55. K. Stamnes, G. E. Thomas, J. J. Stamnes, *Radiative Transfer in the Atmosphere and Ocean* (Cambridge Univ. Press, 2017).

Acknowledgments: ExoMars is a space mission of the European Space Agency (ESA) and Roscosmos. The NOMAD experiment is led by the Royal Belgian Institute for Space Aeronomy (IASB-BIRA), assisted by Co-PI teams from Spain (IAA-CSIC), Italy (INAF-IAPS), and the United Kingdom (Open University). **Funding:** This project acknowledges funding by the Belgian Science Policy Office (BELSPO), with the financial and contractual coordination by the ESA Prodex Office (PEA 4000103401 and 4000121493), by the Spanish MICINN through its Plan Nacional, by European funds under grants PGC2018-101836-B-I00 and ESP2017-87143-R (MINECO/FEDER), and by the Spanish Science Ministry Centro de Excelencia Severo Ochoa Program under grant SEV-2017-0709, as well as by the U.K. Space Agency through grants ST/R005761/1, ST/P001262/1, ST/R001405/1, and ST/S00145X/1 and the Italian Space Agency through grant 2018-2-HH.0. This work was supported by NASA's Mars Program Office under WBS 604796, "Participation in the TGO/NOMAD investigation of trace gases on Mars" and by NASA's SEEC initiative under grant number NNX17AH81A, "Remote sensing of planetary atmospheres in the solar system and beyond." M.J.C. was supported by the NASA Postdoctoral Program at the NASA Goddard Space Flight Center, administered by Universities Space Research Association (USRA) under contract with NASA. S.A. is postdoctoral researcher of the Belgian Fund for Scientific Research (FNRS). **Author contributions:** G.L.V. led the investigation and codeveloped the data analysis and retrieval methods. G.L. codeveloped the analysis and retrieval methods. M.J.C., S.A., E.W.K., I.R.T., and M.A.L.-V. supported with the data analysis and

retrieval methods. A.C.V. led the instrument design/characterization and assisted with the retrievals and data interpretation. F.D., M.D.S., M.J.M., L.N., S.V., M.R.P., J.A.H., G.B., and J.J.L.-M. assisted with the overall planning of the investigation and interpretation of the results. B.R. assisted with the mission planning and coordination of the observations. **Competing interests:** The authors declare that they have no competing interests. **Data and materials availability:** All data needed to evaluate the conclusions in the paper are present in the paper and/or the Supplementary Materials. The retrieval package used in this study is the PSG, free and available online at https://psg.gsfc.nasa.gov. Additional data related to this paper may be requested from the authors.

Submitted 19 May 2020
Accepted 2 December 2020
Published 10 February 2021
10.1126/sciadv.abc8843

Citation: G. L. Villanueva, G. Liuzzi, M. M. J. Crismani, S. Aoki, A. C. Vandaele, F. Daerden, M. D. Smith, M. J. Mumma, E. W. Knutsen, L. Neary, S. Viscardy, I. R. Thomas, M. A. Lopez-Valverde, B. Ristic, M. R. Patel, J. A. Holmes, G. Bellucci, J. J. Lopez-Moreno, NOMAD team, Water heavily fractionated as it ascends on Mars as revealed by ExoMars/NOMAD. *Sci. Adv.* **7**, eabc8843 (2021).